

1 Identifying plausible historical scenarios for coupled lake level  
2 and seismicity rate changes: The case for the Dead Sea during  
3 the last two millennia.

4 **M-Mariana Belferman<sup>1</sup>, A-Amotz Agnon<sup>2</sup>, R-Regina Katsman<sup>1</sup> and Z-Zvi Ben-Avraham<sup>1</sup>**

5 <sup>1</sup> *The Dr. Moses Strauss Department of Marine Geosciences, Leon H. Charney School of Marine  
6 Sciences, University of Haifa, Mt. Carmel, Haifa 3498838, Israel.*

7 <sup>2</sup> *The Fredy & Nadine Herrmann Institute of Earth Sciences, The Hebrew University of  
8 Jerusalem, Jerusalem 9190401, Israel*

9 Mariana Belferman: [mkukuliev@gmail.com](mailto:mkukuliev@gmail.com) (corresponding  
10 author)

11 Amotz Agnon: [amotz@mail.huji.ac.il](mailto:amotz@mail.huji.ac.il)

12 Regina Katsman: [rkatsman@univ.haifa.ac.il](mailto:rkatsman@univ.haifa.ac.il)

13 Zvi Ben-Avraham: [zviba@post.tau.ac.il](mailto:zviba@post.tau.ac.il)

## 14 ABSTRACT

15 Seismicity triggered by water level changes in reservoirs and lakes is usually studied studied  
16 from well-documented contemporary records. Can such triggering be explored on a historical  
17 time scale when the data gathered on water level fluctuations in historic lakes and the earthquake  
18 catalogs suffer from severe uncertainties? These uncertainties stem from the different nature of  
19 the data gathered, methods, and their resolution. In this article, we show a way to considerably  
20 improve the correlation between the continuous recordinterpolated records of historic water level  
21 reconstructions at the Dead Sea and discrete seismicity patterns in the area over the period of the

Formatted: Header & Footer

Style Definition: Normal: Font:

Style Definition: Heading 2: Text Outline

Style Definition: Footer: Font: Font color: Black, Complex Script Font: Arial Unicode MS, (Complex Hebrew

Style Definition: Heading: Text Outline

Style Definition: Hyperlink.3: Font: (Default) Times New Roman, Complex Script Font: Times New Roman, Italian (Italy)

Style Definition: Hyperlink.4: Font: (Default) Times New Roman, 11 pt, Underline color: Custom Color(RGB(31,56,100)), Font color: Custom Color(RGB(31,56,100)), Complex Script Font: Times New Roman, 11 pt, Italian (Italy)

Style Definition: Hyperlink.5: Font: (Default) Times New Roman, 10 pt, Font color: Black, Complex Script Font: Times New Roman, 10 pt

Style Definition: Hyperlink.6: Font: (Default) Times New Roman, 10 pt, Complex Script Font: Times New Roman, 10 pt, Italian (Italy)

Style Definition: Hyperlink.7: Font: (Default) Times New Roman, Complex Script Font: Times New Roman, English (United States)

Style Definition: Hyperlink.8: Font: (Default) Times New Roman, Complex Script Font: Times New Roman, English (United States)

Style Definition: Hyperlink.9: Font: (Default) Times New Roman, Bold, Italic, Font color: Black, Complex Script Font: Times New Roman, Bold, Italic

Style Definition

Style Definition

Style Definition

Style Definition

Style Definition: Comment Text: Font:

Style Definition: Header

Formatted: Body A

Formatted: English (United States)

Formatted: Hyperlink.1

Formatted: Hyperlink.1

Formatted

Formatted: German (Germany)

Formatted: None

Formatted: Centered

Formatted: Header & Footer

22 past two millennia. Constricted Inspired by the data from results of our previous studies study, we  
23 carefully revise the historical earthquake catalog in the Dead Sea keeping only events with  
24 documented destruction in Jerusalem, the largest historical city in the vicinity of the lake. We  
25 then generate an ensemble of random interpolations of water level curves and choose that curve  
26 that best correlates rank them by correlation with the historical records of seismic stress release in  
27 the Dead Sea reflected in the destruction in Jerusalem. We then. We numerically simulate a  
28 synthetic earthquake catalog using this curve. catalog of earthquakes triggered by poroelastic  
29 deformations at hypocentral depths. The catalog is produced by a best-fit water level curve and  
30 by regional strike-slip tectonic deformations. The earthquakes of this synthetic catalog show an  
31 impressing agreement with historic earthquake records from the field. earthquakes documented to  
32 damage Jerusalem. We demonstrate for the first time that a high correlation between water level  
33 changes correlate well with the observed recorded recurrence interval record intervals of  
34 historic earthquakes.

Formatted: Default Paragraph Font

## 35 KEYWORDS

36 Seismic recurrence interval; Water level changes; Effective stress; Dead Sea

Formatted: None

Formatted: Body A

## 37 INTRODUCTION

38 Triggering of earthquakes by water level changes in lakes and reservoirs has been a focus of  
39 seismic investigations conducted all over around the world (e.g. Simpson et al., 1988; Pandey and  
40 Chadha, 2003; Durá-Gómez and Talwani, 2010). #Triggering is attributed to a drop in the effective  
41 normal stress change at a fault, induced by the water level change at the overlying lake's bed  
42 (Simpson et al., 1988; Durá-Gómez and Talwani, 2010; Hua et al., 2013b; Gupta, 2018). This kind

Formatted: Body A

Formatted: Hyperlink.11

Formatted

Formatted: Hebrew

Formatted: Centered

Formatted: Header & Footer

43 of triggering may be particularly significant for areas with moderate and low tectonic strain  
44 accumulations (Pandey and Chadha, 2003; Gupta, 2018), such as the Dead Sea fault in the Middle  
45 East (e.g., Masson et al., 2015).

46 Seismic activity due to water level change was observed beneath artificial reservoirs  
47 immediately after their first filling (e.g. Simpson et al., 1988; Hua et al., 2013 a). It also appeared  
48 after several seasonal filling cycles (Simpson et al., 1988; Talwani, 1997), explained by diffusion  
49 of pore pressure diffusion to the earthquake's hypocentral depth via the fault (Durá-Gómez and  
50 Talwani, 2010). The correspondence of this kind of contemporary seismicity to water level change  
51 is usually identified based upon real-time data.

Formatted: Hebrew

52 Alternatively, on a much longer time scale, changing seismic activity may also be associated  
53 with water level changes in historic water bodies (e.g., the Dead Sea, 4since 2 ka present, Fig. 1A,  
54 in Appendix, which occupies the tectonic depression along the Dead Sea fault). Water level hikes  
55 of ~15 m, characteristic for time intervals of centuries to millennia, were analysedanalyzed in  
56 Belferan et al., (2018) and shown to be able to moderately representmoderate the seismicity  
57 pattern at the Dead Sea fault (Belferan et al., 2018).

Formatted: None

Formatted: None

58 However, reconstruction of fluctuations in historic lake levels and the concurrent seismicity  
59 are both includesubject to significant uncertainties. They stem from the differing nature of the data  
60 gathered on these two phenomena, and thus deserve special consideration. Earthquake dating can  
61 be quite precise, and its accuracy can beis verified when different historical sources show  
62 consensus (Guidoboni et al., 1994; Guidoboni and Comastri, 2005; Ambraseys, 2009). Assessment  
63 of the extent of damage (hence earthquake magnitude), similarly requires such a consensus  
64 between the different data sources. Sediment records can help to calibrate the analysis of the

Formatted: Centered

65 historical evidence (Agnon, 2014; Kagan et al., 2011). Such records can be tested by trenching  
66 ([KlingerWechsler](#) et al., [2015](#)[2014](#); [Marco and Klinger, 204](#); Lefevre, 2018). However, in many  
67 cases [location of the](#) earthquake epicenter can be imprecise or not even known. [Consequently](#),  
68 [considerable uncertainty pertains to the historical catalog of earthquakes related directly to the](#)  
69 [Dead Sea](#).

70 By contrast, [historic](#)[historical](#) water level records are quite precise [elevation wise](#), as they  
71 are obtained from different points around the lake (Bookman et al., 2004; Migowski et al., 2006).

72 However, water level dating could have an error of about  $\pm 45$  yr, as estimated from the radiocarbon  
73 dating of shoreline deposits in [a](#)-fan delta [outcrop](#)[outcrops](#) (Bookman et al., 2004). This may  
74 underestimate the actual dating uncertainty due to reworking of organic matter, sometimes re-  
75 deposited a century or more after equilibration with the atmosphere (Migowski et al., 2004). In  
76 addition, the entire past bi-millennial Dead Sea level record is constrained by less than twenty  
77 “anchor points” (the data obtained by the dating collected from surveyed paleo-shorelines,  
78 Bookman et al., 2004). Therefore, its continuous reconstruction, as suggested in the literature  
79 (Migowski et al., 2006; Stern, 2010), usually takes different forms within the acceptable limits  
80 dictated by the limnological evidence (Bookman et al., 2004). A challenging uncertainty for our  
81 study arises from [the interpolations required for](#) periods when the available data does not constrain  
82 the water levels.

83 In this article, we take advantage of the correlation between the historic water level  
84 reconstructions at the Dead Sea and seismicity patterns in the area over the past two millennia. We  
85 demonstrate for the first time that plausible scenarios for the lake level history can fit very well  
86 the record of the historic [earthquakes](#) [RI](#). [The fit can even be improved when moderate local](#)  
87 [earthquakes are considered for stress release history](#)[earthquake recurrence intervals \(RIs\)](#). Based

88 on the correlation between these phenomena, we offer an alternative explanation regarding the  
89 triggering of the earthquakes in the area of the Dead Sea.

Formatted: Header & Footer

## 90 METHODS

91 To investigate the relation between an accurate but discrete chronology of earthquakes and  
92 the continuous water level (WL) change, we first explore the space of possible WL histories by a  
93 statistical approach. We generate an ensemble of WL curves (based on the anchor points  
94 (Bookman et al., 2004), while remaining within the limits dictated by climatic and morphological  
95 constraints (Bookman et al., 2004; Migowski et al., 2006 and Stern, 2010), by using a random  
96 number generator.

### 97 BestA best fit random method of WL curve prediction

98 The compilation of WL curves of the Dead Sea for the last two millennia from three recent  
99 publications (Bookman et al., 2004; Migowski et al., 2006 and Stern 2010) is presented in Figure  
100 1A by dashed linescurves. Generally, the differences between all dashed curves at anchor points  
101 is included within an error limit of  $\pm 45$  yr as indicated by error bars, with thean exception of the  
102 anchor point dated to 1400 CE (Bookman et al., 2004) for which Migowski et al. (2006) and Stern  
103 (2010) suggested a higher WL. Nevertheless, each hypothetical WL curve is forced to pass through  
104 all anchor points according to Bookman et al. (2004) except for one, at around 500 CE. The WL  
105 drop around this time, according to Migowski et al. (2006) and Stern (2010), occurred later than  
106 was originally suggested by Bookman et al. (2004) (Figure 1A). Because this  
107 shift is within the permissible error limits ( $\pm 45$  yr), this anchor point is shifted to the left (+40 yr).  
108 In addition, the WL determined on the curve edges of the studied bi-millennial time interval was  
109 fixeddefined by antwo anchor points, through which the estimated WL curve passed

Formatted: None

Formatted: German (Germany)

Formatted: Body A

Formatted: Body A, Justified, Indent: First line: 0 cm, Space Before: 12 pt, After: 8 pt, Line spacing: Double

Formatted: Font: Bold

Formatted: Hyperlink.0

Formatted: Body A

Formatted: English (United States)

Formatted: None

Formatted: None

Formatted: None

Formatted: None

Formatted: None

Formatted: English (United States)

Formatted: None

Formatted: Centered

110 according to all three references ~~specified above~~. In total, we have 13 anchor points. Between  
111 each pair of points, the ~~trend~~trends in the WLs ~~is~~are constrained by the sedimentary facies  
112 (Migowski et al., 2006) that specify the edge points of the interval as the extrema for the acceptable  
113 WL variation.

114 However, within the largest interval between the anchor points (600 - 1100 CE), the ~~on-~~  
115 ~~landfield~~ studies (Migowski et al., 2006; Stern, 2010; Bookman et al., 2004) constrained the WL  
116 to be lower than the extrema at the edges of that interval. For this period, the WL was randomly  
117 interpolated between ~~the suggested maximum (higher (e.g., Migowski et al., 2006) and~~  
118 ~~minimum lower (e.g., Stern, 2010) bounds~~. To maintain a monotony of the WL variation,  
119 ~~(required by the facies analysis of Migowski et al.)~~, a moving average filtered the random noise  
120 between every pair of anchor points. Accounting for the above-mentioned limits, and setting a ten-  
121 year step, the model ~~generates~~has generated 10 ~~Million~~million WL curves for the last bi-millennial  
122 interval, using a uniformly distributed random number generator.

123 ~~The~~We test for linear correlation between the recurrence intervals (RIs) of the widely  
124 recorded moderate-to-large ( $M > 5.5$ ) historical earthquakes available from the literature (see Table  
125 1 and the text description in Appendix), and the generated WLs, ~~was tested (e.g., WL interpolations.~~  
126 ~~The test is given~~ (as in Figure 9 in Belfer et al., 2018) by ~~calculating~~ the value of the Pearson  
127 product-moment correlation coefficient, R (Figure 2B1B). We use ~~these statisticsthis statistic~~ for  
128 evaluating the suitability of each randomly interpolated WL curve for our analysis, for  
129 identification and elimination of any outliers, and for studying the behavior of the entire ensemble  
130 of the curves generated.

### 131 The earthquake simulation algorithm

Formatted: Header & Footer

Formatted: None

Formatted: Centered

132 The most suitable WL curve suggested by this correlation (discussed in the results section  
 133 below), was used to generate a “[Synthetic](#)” earthquake [synthetic](#)” earthquake catalog based on the  
 134 algorithm described in this section. [Synthetic](#) earthquakes are simulated in the model by  
 135 superimposing the [effective](#)[Effective](#) normal [poroelastic](#) stress change due to the WL change [is](#)  
 136 [superimposed](#) on the tectonic stress accumulated [consistently with the slip rate](#) since the preceding  
 137 seismic event, [and synthetic](#) earthquakes are simulated using a Coulomb failure envelope and a  
 138 [Mohr](#) circle (Jaeger et al., 2009). A vertical outplane strike-slip fault below the lake/reservoir bed  
 139 is assumed (simulating a Dead Sea fault), embedded in 2D (plain strain) geometry of the upper  
 140 crust (see Belferma et al., 2018). Tectonic horizontal strike-slip displacements at the fault are  
 141 approximated by a simple shear approach with no normal strain component.

142 In the [poroelastic](#) part of the model, horizontal stress change normal to the strike slip fault  
 143 produced by the water level change, is calculated under a uniaxial (vertical) strain condition  
 144 (Eq.10b in Belferma et al., 2018), applicable to a post-diffusion stage: i.e., when pore pressure at  
 145 hypocentral depth approaches that at the lake’s bed. An array of [WL](#) change,  $\Delta h_i$  ( $i = 1, 2, \dots, 2000$ ), was generated. Using this array, another array of the effective normal stress changes,  
 146  $\Delta \sigma'_i$ , at the fault, induced by water load change at the lake’s bed,  $p_{s_i}$ , is calculated as  $p_{s_i} \Delta$   
 147 corresponds to the array of the [WL](#) change,  $\Delta h_i$  ( $i = 1, 2, \dots, 2000$ ) over the interpolated water level  
 148 curve, Figure 1D:

$$1. \quad \Delta \sigma'_i = \frac{1-2\nu}{1-\nu} (\beta - 1) p_{s_i}$$

150  
 151 (see Eq. 10b in Belferma et all., 2018). [This equation assumes the post diffusion stage: i.e. when](#)  
 152 [pore pressure at the hypocentral depth approaches the value at the lake’s bed](#). Here  $\beta$  is Biot’s

Formatted: Header & Footer

Formatted: Font color: Auto  
 Formatted: None, Font color: Auto  
 Formatted: Font color: Auto  
 Formatted: None, Font color: Auto

Formatted: Body A  
 Formatted: None, Font color: Auto  
 Formatted: None, Font color: Auto,  
 Formatted: None, Font color: Auto  
 Formatted: None, Font color: Auto,  
 Formatted: None, Font color: Auto  
 Formatted: None, Font color: Auto

Formatted: Hyperlink,0, Font: Not Italic, Font color: Auto  
 Formatted: Font color: Auto  
 Formatted: Hyperlink,0, Font: Not Italic, Font color: Auto  
 Formatted: None, Font color: Auto  
 Formatted: Centered

153 coefficient and  $\gamma$  is the Poisson's ratio,  $p_{si} = \rho g \Delta h_i$ , where  $\rho$  is the density of water and  $g$  is the  
154 acceleration of gravity.

155 [A radius and a centre location of the Mohr circle change as a function of tectonic deformations](#)  
156 [and water level changes, correspondingly, eventually reaching a failure envelope that simulates an](#)  
157 [earthquake.](#) The model uses a Byerlee's law envelope (Byerlee, 1978) to define the [residual](#)  
158 strength of a seismogenic zone at the fault immediately after the earthquake (see Belferan et al.,  
159 2018 for more detail). [Since the effective stress upon the onset of an earthquake is specified by a](#)  
160 [high failure envelope and the effective stress following the slip is given by the Byerlee law, the](#)  
161 [model is time-predictable. The stress drop, at least in the nucleation zone, is expected to be](#)  
162 [proportional to the recurrence interval.](#)

163 The starting point of the simulations is the date of the first historic earthquake (33CE, see  
164 Table 1 in the Appendix) from the [studied](#) bi-millennial time interval [studied](#). The simulation  
165 incrementally proceeds with time over the [chosen](#) WL curve [generated](#) (as above) [also](#)  
166 [considering under](#) the [accumulating](#) tectonic stress [accumulation](#). After each stress release, the  
167 time to the next earthquake,  $\Delta t$ , is calculated [using from](#) the solution of the Mohr-Coulomb failure  
168 criterion for a strike-slip tectonic regime [and a WL change](#),  $\Delta h_i$ , applicable to the Dead Sea fault  
169 (Belferan, et al., 2018):

$$2. \quad (\tau_i - \tau_0)^2 + (\sigma_i - (\sigma_0 + \Delta\sigma'_i))^2 = (R_0 + \Delta\tau_{xy_i})^2$$

$$\tau_i = C + \tan(\varphi)\sigma_i$$

170 assuming that  $\Delta\tau_{xy_i} = \frac{C \cos(\varphi)}{t_{RI}} \Delta t$  is the tectonic shear stress [accumulated consistently with slip-](#)  
171 [rate](#) at the strike-slip fault [accumulated](#) during the period  $\Delta t$  (time passed since the last earthquake),

		Formatted: Header & Footer
174	$C$ is cohesion, $\varphi$ is an angle of internal friction, $\sigma_0$ and $\tau_0$ are the coordinates of the Mohr circle	Formatted: Font color: Auto
175	immediately after the earthquake and $R_0$ its radius, $t_{RI}$ is the reference RI corresponding to the	Formatted
176	minimal WL.	Formatted
177	For each time step, the algorithm determines whether there is a single solution, or two, or <del>no</del>	Formatted
178	<del>solutions</del> <a href="#">nil</a> . A case of no solutions means that the Mohr circle is yet to reach the failure envelope,	Formatted
179	as the <del>accumulated</del> <a href="#">accumulating</a> tectonic stress and the WL increase are still insufficient. The	Formatted
180	system of Eq. 2 may have <del>one</del> <a href="#">single</a> solution when <del>an</del> <a href="#">the</a> earthquake occurs at the end of some	Formatted
181	<del>step in time</del> <a href="#">timestep</a> , or two solutions when the failure criterion is met before the end of the <del>time</del>	Formatted
182	<del>step</del> <a href="#">timestep</a> . A case of two solutions is rounded down to a case of a single solution <del>if</del> <a href="#">if</a> a time	Formatted
183	step (one year) is small compared to the earthquake RI (several hundreds of years).	Formatted: None, Font color: Auto
184	This solution of Eq.2 yields a RI as a function of the effective normal stress change, $\Delta\sigma'_i$	Formatted: Font color: Auto
185	(Belferman et al., 2018):	Formatted
186	3. $RI = \Delta t = (C + \tan(\varphi)\Delta\sigma'_i) \frac{t_{RI}}{c}$	Formatted
187	where $t_{RI}$ is the reference <a href="#">RI</a> <a href="#">corresponding</a> <a href="#">RI</a> <a href="#">corresponds</a> to the minimal WL, $C$ is cohesion, $\varphi$ is	Formatted: Hyperlink,0, Font: Not Italic, Font color: Auto
188	an angle of internal friction. From this formula for $RI$ , <a href="#">the</a> <a href="#">an</a> array of earthquake dates is obtained.	Formatted
189	Substituting Eq.1 into Eq.3, we get a simulated RI as a linear function of WL change with time,	Formatted
190	$\Delta h_i$	Formatted
191	4. $RI = t_{RI} + \frac{\tan(\varphi) 1-2\nu}{c} (\beta - 1) \rho g t_{RI} \Delta h_i$	Formatted
192	Coefficients for the simulations were previously determined in Belferman et al. (2018). <a href="#">Note that</a>	Formatted: Hyperlink,0, Font: Not Italic, Font color: Auto
193	<a href="#">the cohesion</a> $C$ <a href="#">is not a-priory</a> <a href="#">known</a> <a href="#">hence it is fixed by the empirical correlation between WL</a>	Formatted: None, Font color: Auto
194	<a href="#">and RI for a given lake level history considered</a> . In addition, <a href="#">a left lateral strike</a> <a href="#">the</a> <a href="#">slip</a> <a href="#">tectonic</a>	Formatted: Centered

195 motion-rate is set at the Dead Sea fault with a constant velocity of  $5 \text{ mm/yr}$  (e.g. Hamiel et al.,  
196 2018; Hamiel and Piatibratova, 2019; Masson et al., 2015) is used.). The change in WL is  
197 calculated relative to its minimal level (415 m bmsl) over the period. A cohesion value,  $C =$   
198  $0.08 \text{ MPa}$  and a reference RI,  $t_{RI} = 300 \text{ yr}$ , were adjusted numerically for a specific WL curve,  
199 providing the average RI of 144 yr over the modelled period of two millennia justified by  
200 historical, archaeological, and geological data (Agnon, 2014).

## 201 RESULTS

202 The best fit WL curve (black solid line in Figure 1A) was Ten most suitable WL curves  
203 (Figure 2) are identified out of the 10M random set of WL randomly generated curves  
204 (“ensemble”) by the Pearson product-moment correlation test. The values of correlation  
205 coefficients, R, for the entire ensemble of randomly interpolated WLs are distributed normally  
206 around  $R=0.63$  (Figure 1B) with a standard deviation of  $\sigma = 0.076$ .

207 Three outliers from the thirteen RIs of the widely recorded historic earthquakes (749 CE,  
208 1293 CE, 1834 CE in Figure 1) were identified and reevaluated (Figure 1D(see the explanation in  
209 Appendix). A curve with a highest Pearson coefficient of  $R=0.912$  was chosen from the correlation  
210 between the RIs of the revised historic catalog and the randomly generated WLs. This correlation  
211 can be specified by a linear prediction function

$$212 5. \quad RI = -5442 - 14WL$$

213 where RI is given in years and WL in meters. In addition, a synthetic earthquake history including  
214 14 seismic events was simulated from the chosen best fit randomly interpolated WL curve with

Formatted: Header & Footer

Formatted: None, Font color: Auto  
Formatted: Font color: Auto  
Formatted: None, Font color: Auto  
Formatted: Font color: Auto  
Formatted: None, Font color: Auto

Formatted: German (Germany)

Formatted: Body A

Formatted: Hyperlink.5  
Formatted: Hyperlink.5  
Formatted: Hyperlink.5  
Formatted: Hyperlink.5  
Formatted: Hyperlink.5, Pattern: Clear  
Formatted: Hyperlink.5  
Formatted: Font: 14.5 pt  
Formatted: Hyperlink.5  
Formatted: None  
Formatted: None  
Formatted: English (United States)  
Formatted: None  
Formatted: None, Pattern: Clear (White), Not  
Formatted: None  
Formatted: None  
Formatted: Hyperlink.0, Font: Not Italic

Formatted: None

Formatted: None

Formatted: Centered

215 R=1 specified above. The correlation between the synthetic RIs and WLs (presented in [Figure](#)

Formatted: Header & Footer

216 [Figure 1C](#)) is:

Formatted: None

Formatted: None

217 6.  $RI = -3840 - 10WL$

Formatted: Hyperlink,0, Font: Not Italic

218 as expected from the linear dependence suggested by the analytical solution (Eq.4). The dates of  
219 the simulated synthetic earthquakes are presented, versus the dates of the historic earthquakes from  
220 the literature (Table A1, Appendix) in [Figure](#) [Figure](#) 1E.

Formatted: None, Font color: Auto

Formatted: Font color: Auto

Field Code Changed

Formatted: Font color: Auto

Formatted: None, Underline color: Custom Color(RGB(31,56,100)), Font color: Auto

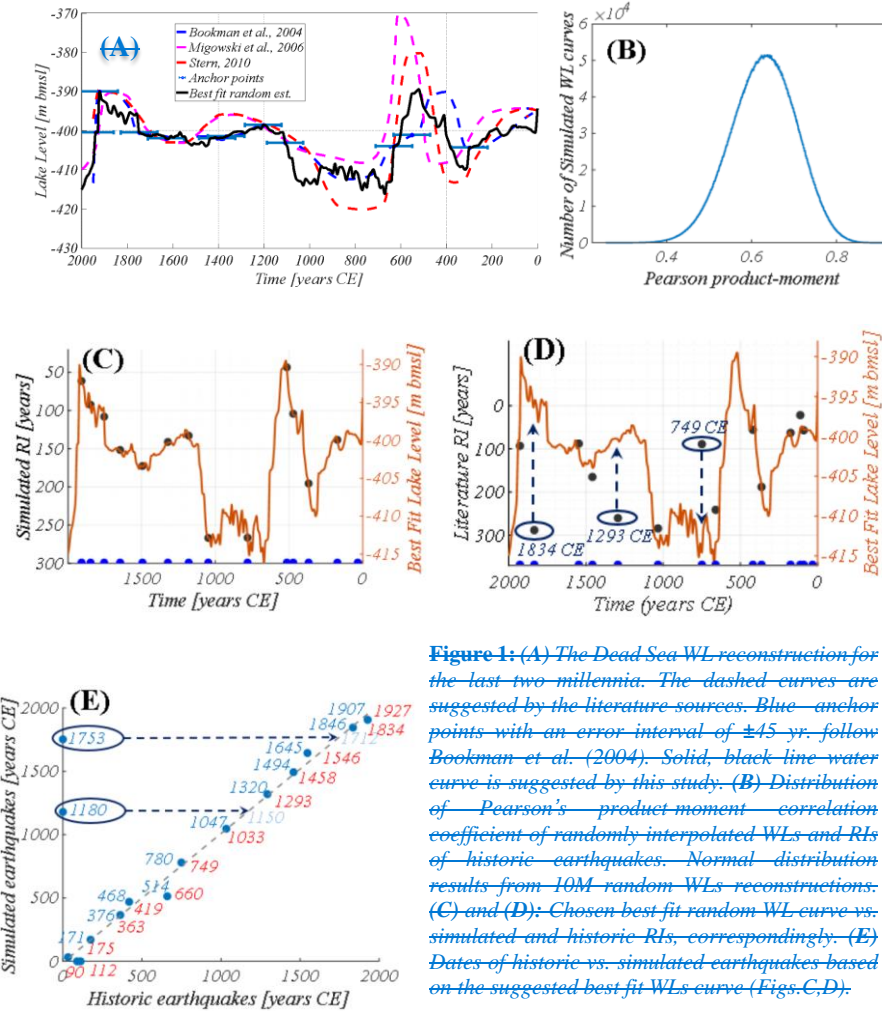


**Figure 1:** (A) The Dead Sea WL reconstruction for the last two millennia. The dashed curves are suggested by the literature sources. Blue anchor points with an error interval of  $\pm 45$  yr. follow Bookman et al. (2004). Solid, black line water curve is suggested by this study. (B) Distribution of Pearson's product moment correlation coefficient of randomly interpolated WLs and RLs of historic earthquakes. Normal distribution results from 10M random WLs reconstructions. (C) and (D): Chosen best fit random WL curve vs. simulated and historic RLs, correspondingly. (E) Dates of historic vs. simulated earthquakes based on the suggested best fit WLs curve (Figs. C,D).

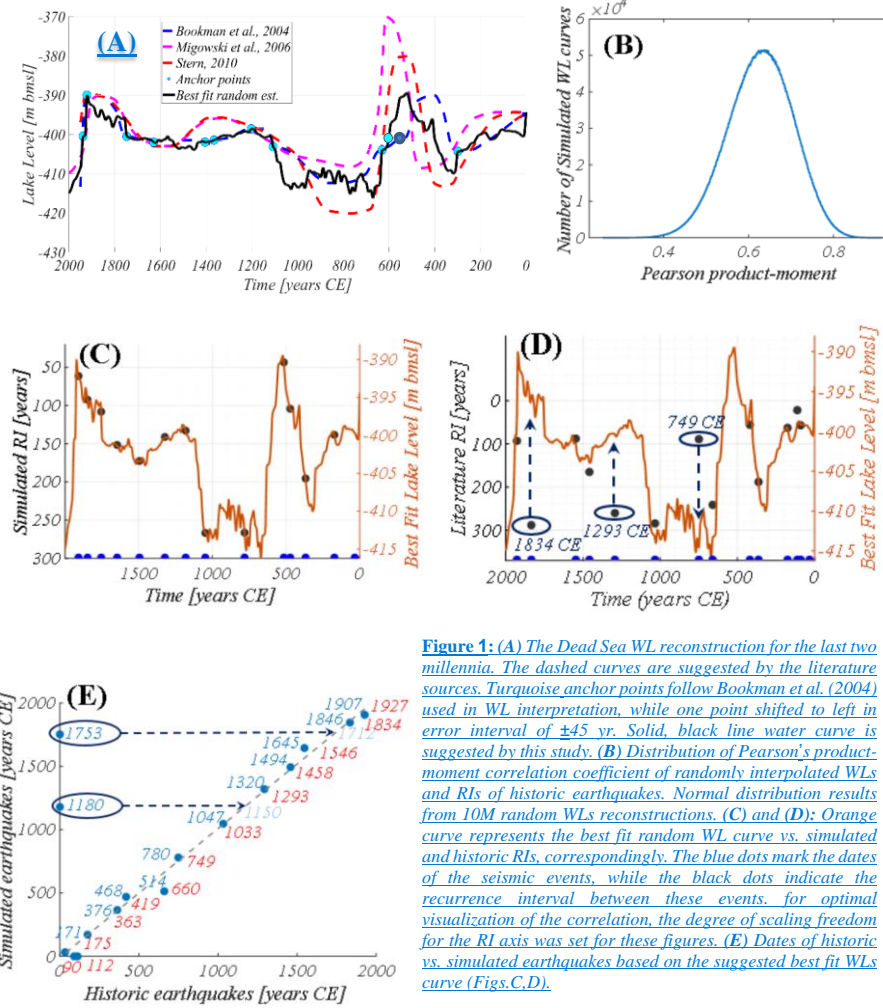


**Figure 1:** (A) The Dead Sea WL reconstruction for the last two millennia. The dashed curves are suggested by the literature sources. Turquoise anchor points follow Bookman et al. (2004) used in WL interpretation, while one point shifted to left in error interval of  $\pm 45$  yr. Solid, black line water curve is suggested by this study. (B) Distribution of Pearson's product-moment correlation coefficient of randomly interpolated WLs and RIs of historic earthquakes. Normal distribution results from 10M random WLs reconstructions. (C) and (D): Orange curve represents the best fit random WL curve vs. simulated and historic RIs, correspondingly. The blue dots mark the dates of the seismic events, while the black dots indicate the recurrence interval between these events. For optimal visualization of the correlation, the degree of scaling freedom for the RI axis was set for these figures. (E) Dates of historic vs. simulated earthquakes based on the suggested best fit WLs curve (Figs.C,D).

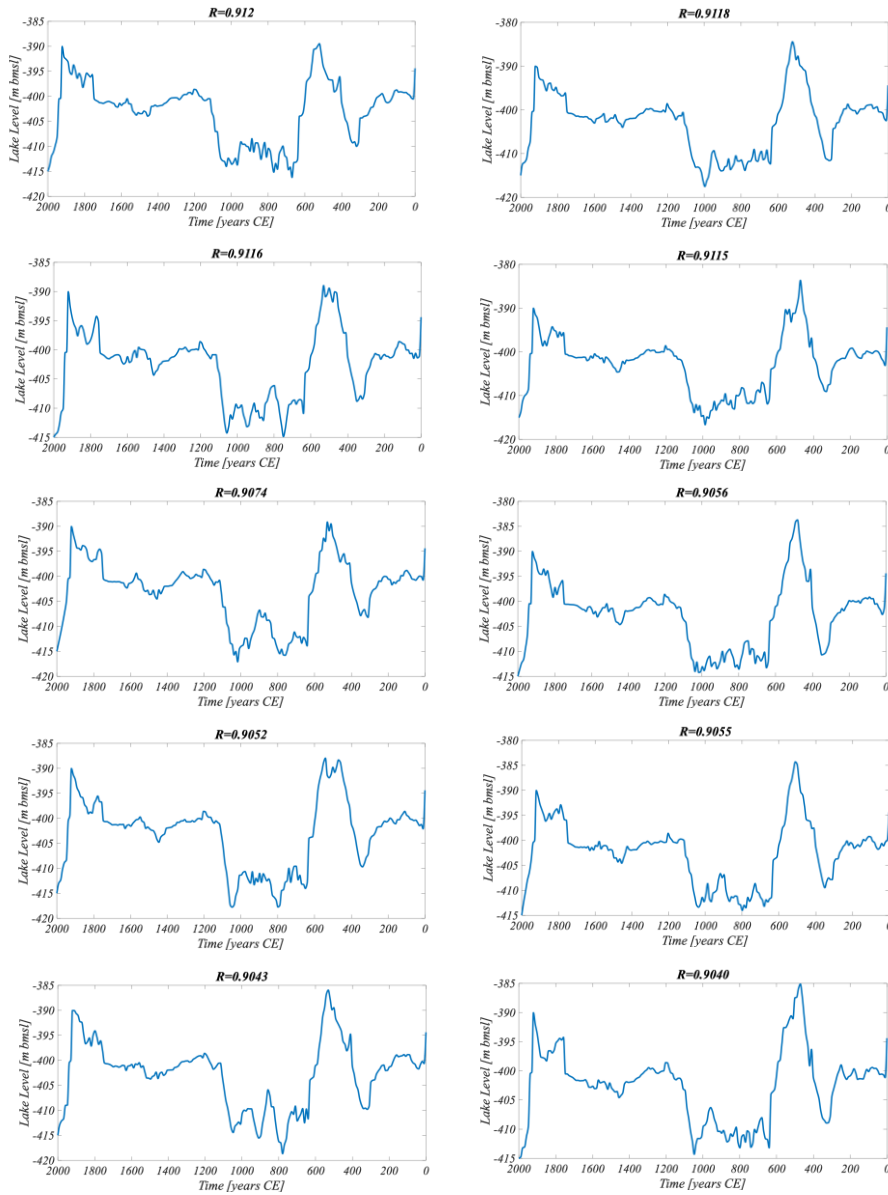


Figure 2: Ten most suitable WLs identified out of the 10M randomly generated by the Pearson product-moment

225 **DISCUSSION**

226 Uncertainties in the WL reconstructions associated with dating and resolution lead to  
227 considerable variance in possible interpolations ([Figure 1B](#)–[Figure 1B](#)). A Pearson correlation  
228 coefficient test shows that most of the randomly interpolated WL curves give linear correlation  
229 with earthquake RIs (indicated by a mean Pearson coefficient of  $R=0.63$ ), excluding the three  
230 outliers ([Figure 1D](#) to be discussed below) to be discussed below. [Figure 2](#) shows a  
231 similar pattern of the WL change for the ten most correlated curves. In all cases, a significant rise  
232 in the water level of about 400 CE and 1100 CE is visible and a decrease in the WL around 200  
233 and 600 CE. Also, the maximum level around 500 and 1900 CE appears in all ten cases.

234 For simulating synthetic earthquakes triggered by WL change, we use the WL curve that  
235 generates the highest correlation with the revised historical catalog ( $R = 0.912$ ). The dates of these  
236 simulated synthetic earthquakes are comparable with historical earthquakes ([Figure 1E](#)–[Figure 1E](#))  
237 excluding two events, whose [dates](#) [date labels](#) are [shifted](#) [offset](#) to the y-axis for clarity of  
238 presentation (1753 CE, 1180 CE). The dates of these synthetic earthquakes might be connected to  
239 three outliers from the historical catalog (1834 CE, 1293 CE, 749 CE depicted in [Figure 1D](#)–[Figure](#)  
240 [1D](#)) as explained below.

241 The 1180 CE synthetic earthquake ([Figure 1E](#)–[Figure 1E](#)) is comparable to an earthquake in  
242 the literature dated by Ben-Menachem (1979) and Amiran et al. (1994) to the mid-12th century  
243 (~1150 CE). Ambraseys (2009) doubted the precise dating but accepted this mid-12th century  
244 estimate. The damaged area of this earthquake spanned Jericho and Jerusalem, and the event could  
245 be considered as significant, because it led to the total destruction of two monasteries, one of which  
246 is 10 km south of Jerusalem's curtain wall. By admitting the ~1150 CE earthquake to the amended

Formatted: Header & Footer

Formatted: German (Germany)

Formatted: None

Formatted: Body A

Formatted: None

Formatted: None, English (United States)

Formatted: None

Formatted: None

Formatted: None, Font: (Default) Times New Roman

Formatted: None

Formatted: None

Formatted: Centered

catalog, we reduce the RI of the subsequent earthquake at 1293 CE (Figure 1D) from 247 260 to 143 yrs, thereby bringing this outlier very close to the linear correlation. 248

Our model also generates an earthquake in the 18th century, dated 1753 CE, for which there 249 250 were no matches in our initial historical catalog (Belferman et al., 2018). However, in Amiran's 251 et al. (1994) catalog an earthquake in 1712 CE is indicated: 'The quake shook the solid houses and 252 ruined three Turkish houses. Felt in Ramle, but not in Jaffa'. Additionally, this earthquake is 253 evidenced by seismites dated to 1700 – 1712 CE from an Ein Gedi site (Migowski et al., 2004).

Regarding the modeled 1907 CE event, we note the well documented (although often 254 255 overlooked) 29 March 1903 CE earthquake (Amiran et al., 1994). This was a moderate but 256 extendedprolonged earthquake: local intensity reached VII in a number of localities distributed 257 outside the rift valley over an area of 140x70 square km (including Jerusalem), whereas the 258 maximum intensity reported in the rift was VII as well (Jericho). We prefer to correlate the 259 modeled 1907 event with the stronger 1927 Jericho earthquake that clearly released stress in the 260 Dead Sea (e.g. Shapira, et al., 1993; Avni et al., 2002; Agnon, 2014). This leaves the 1903 261 unmatched to our model. Perhaps the earthquake ruptured the northern part of the central Jordan 262 Valley, north of the Dead Sea and south of Lake Kinneret (Sea of Galilee).

Regarding the last outlier from the historical earthquakes dated to 749 CE (or its neighbors 263 264 747 and 757, Table A1 in the Appendix) (Figure 1D) and corresponding to the simulated 265 266 780 CE earthquake (Figure 1E): the simulation generated the preceding earthquake 514 267 268 CE associated with the 659/660 CE event from the literature (Table A1 in the Appendix) with a deviation of 146 years. The rupture zone of 659/660 CE event is uncertain, and this earthquake is not necessarily related to stress release at the Dead Sea basin. Alternatively, following

269 [RusselRussell](#) (1985), as a result of the 551 CE earthquake, a [fortressesfortress](#) east of the southern  
270 Dead Sea and Petra were destroyed. Newer data ([Mareo et al., 1996](#)) contradicts the assertion  
271 regarding Petra; a failure at the Dead Sea region is still plausible. Replacing the 660 CE earthquake  
272 with 551 CE in the [list of relevant historical earthquakescatalog](#) changes the RI preceding the 749  
273 CE historical earthquake from 89 to 198, which brings this outlier into a satisfactory linear  
274 correlation ([Figure 1D](#)[Figure 1D](#)).

Formatted: Header & Footer

275 Additionally, it should be emphasized that in the simulation presented in this article, the  
276 starting point is, quite arbitrarily, the earthquake of 33CE. This event [andtogether with](#) the  
277 subsequent earthquakes 90CE and 112CE (not predicted by our model) span a single century-  
278 [where the catalog is nebulous](#). Each of these events could thus represent the starting point of the  
279 simulations, or could be omitted at this early and poorly documented interval.

Formatted: None

280 Summarizing the above amendments, we add to our [listcatalog](#) of historic events the 551  
281 CE, ~1150 CE, 1712 CE, earthquakes and remove 559/660 CE and 90CE, 112 CE earthquakes  
282 (Figure 1E). Altogether, we get 14 triggered historic earthquakes.

Formatted: None

283 The [RI of the resulting list of historical earthquakes linearly correlates with WL change](#).  
284 [Thiscorrelation between the water level and recurrence interval](#) is noticeable [despitefor](#) the  
285 [different formvarious variants](#) of the water level [curvescurve reconstruction](#) (Figure 23).

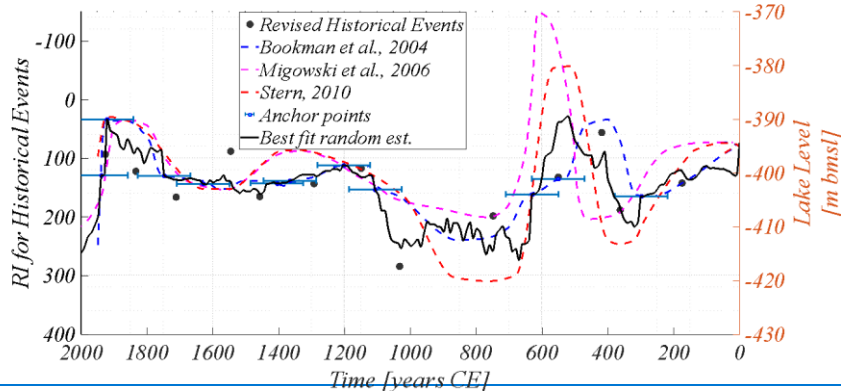
Formatted: None

Formatted: None

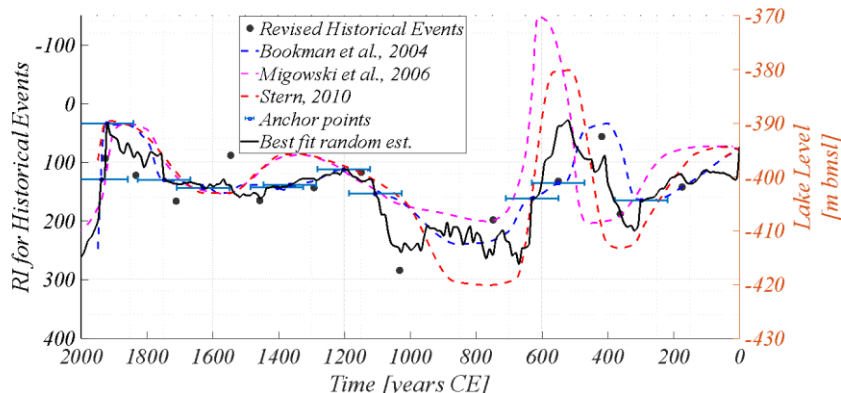
Formatted: None

Formatted: None

Formatted: None



286



287

288 **Figure 23:** The Dead Sea WL reconstruction for the last two millennia. The dashed curves are suggested  
 289 by the literature. Blue anchor points with an error interval of  $\pm 45$  yr follow Bookman et al. (2004). The  
 290 solid black line is the water level curve suggested by this study. The black points represent the RI for revised  
 291 historical events, suggested in this study as being relevant to the Dead Sea area.

Formatted: Font color: Black

Formatted: Body A

Formatted: Font: Not Italic, Font color: Black, Complex Script Font: Not Italic, Hebrew

Formatted: Font color: Black

Formatted: Font color: Black

292 The correlation of RI with best fit random estimated curve can be specified by a linear  
 293 prediction function:

Formatted: Centered

294      7.  $RI = -2483 - 6.5WL$

295      This linear relationship between WL and RI underscores the previously proposed  
 296      correlations between these phenomena (in Figure 9 in Belferman et al., 2018).

297      Since the last earthquake (1927CE), the water level in the Dead Sea has continuously  
 298      decreased at an average annual rate of ~1 m/yr. Today the water level is about -440 (m bmsl), thus  
 299      our prediction function ~~suggests~~suggests an RI of 377 yr, for such a WL. [More](#)  
 300      [specifically](#)[Alternatively](#), if the water level in the Dead Sea ~~remained~~should remain constant (-440  
 301      m bmsl), [as intended in some mitigation plans](#), we would expect the next earthquake at about  
 302      ~2300 yr. [However, as the water level keeps falling, a moderate to large earthquake is predicted](#)  
 303      [even later](#).

304      This paper stresses that reconstructions of WL curves are not unique and may take various  
 305      forms under the constraints available (e.g., [Figure 1A](#)). However, the correlation with an  
 306      independent record of RIs of seismic events, assuming that earthquakes are affected by WL hikes,  
 307      allows deciphering plausible scenarios for WL evolution. Moreover, for cases with the best but  
 308      not perfect correlation, the deviation might be consistent with a release of elastic energy by smaller  
 309      earthquakes, which are not accounted for by the deterministic part of our model. We note that  
 310      smaller earthquakes might rupture ~~dipping~~[dip-slip](#) fault planes, again not accounted for by our  
 311      simple model.

312      [Additionally, as large earthquakes are accompanied by aftershocks, some of the elastic](#)  
 313      [energy is released by them. Moreover, it was shown earlier, in areas where earthquakes caused by](#)  
 314      [artificial reservoirs, how this mechanism influenced by water level change. It was shown that in](#)  
 315      [areas of induced seismicity, earthquakes are not only accompanied by aftershocks but also](#)

Formatted: Header & Footer

Formatted: Hyperlink,0, Font: Not Italic

Formatted: Hyperlink,0, Font: Not Italic

Formatted: None

Formatted: Body A

Formatted: None, English (United States)

Formatted: None

Formatted: Centered

316 preceded by foreshocks (Gupta, 2011). The decay curve of this kind of seismicity satisfies criteria  
317 for the second class of earthquake sequences by Mogi (1963). The lack of instrumental records of  
318 historical earthquakes in our study area, does not allow comparison with this class. The 1995 Gulf  
319 of Aqaba earthquake (7.2 Mw), the last instrumentally recorded earthquake, was accompanied by  
320 a long period (significant enough for stress release consideration) of aftershocks. The earthquake  
321 occurred along the southern part of the plate boundary, which is far enough from the Dead Sea,  
322 and most likely is not influenced by the water level change. Following this earthquake, felt  
323 aftershocks continued for about two years. At least 50 percent of the total moment associated with  
324 these aftershocks was released during the first day after the main shock and over 95 percent in the  
325 first 3 months (Baer 2008). In total, the post-seismic moment released during the period of 6  
326 months to 2 yr after the Nuweiba earthquake is about 15 percent of the co-seismic moment release  
327 (Baer 2008). This earthquake showed that the response of the crust to earthquakes by aftershocks  
328 is negligible, as noted for many large earthquakes (e.g., Scholz 1972).

329 For the case of artificial reservoirs, it was shown that for induced seismicity sequences,  
330 aftershocks continue for a longer time than for tectonic earthquake sequences (Gupta, 2011).  
331 However, because the time scale of RI, the period of aftershocks is insufficient to consider  
332 earthquakes from the sequence in our model as separate events. Regarding the time scale presented  
333 in our study, when the minimal inter-seismic period is about 50 years, the stress released during  
334 post -seismic period can be considered a part of the main shock.

335 The mechanical model used in this article is rather simplistic, where earthquakes release  
336 strike-slip loading. The basins around the Dead Sea fault system testify for also an extensional  
337 component that could be manifested in co-seismic motion along normal faults. To justify our focus  
338 on a single type of fault (strike-slip), we list the following arguments:

339     • The far-field maximal and minimal principal stresses in the Dead Sea region are horizontal  
340           (Hofstetter et al., 2007; Palano et al. 2013). This is compatible with a dominance of strike-  
341           slip faulting (Anderson, 1951). The tectonic motion at the DSF is characterized  
342           predominantly by a left-lateral strike-slip regime with a velocity of ~5 mm/yr along various  
343           segments (Garfunkel, 2014; Masson et al., 2015; Sadeh et al., 2012). Large earthquakes that  
344           initiate clusters are likely to rupture along the straight ~100 km strike-slip segments  
345           (Lyakhovsky et al., 2001). The strike of these segments parallels the relative plate velocity  
346           vector and thus can be approximated by a simple shear. Additionally, in the Dead Sea basin,  
347           GPS surveys indicate dominance of strike slip loading. Hamiel et al. (2018) show that, on  
348           a plate scale, horizontal shear loading dominates the velocity north of the lake. Hamiel and  
349           Piatibratova (2019) detected a sub mm/yr component of extension across the southern  
350           normal fault bounding the Dead Sea pull apart, yet the strike-slip component across this  
351           very fault seems much larger.

352     • Normal, as well as strike-slip faults, similarly react to water level change that contributes  
353           to the vertical stress component and pore pressure change. The seismicity induced by  
354           surface water level fluctuations and affected by the faulting regime is critically determined  
355           by the relative orientations of the three principal stresses (Anderson, 1951). In regions  
356           where the vertical compressive stress is not minimal (normal and strike-slip faulting),  
357           seismic activity is more sensitive to the effective stress change due to water level change,  
358           than in regions where it is minimal (thrust faulting) (Simpson, 1976; Snow, 1982; Roeloffs,  
359           1988). This is applicable to a case of reservoirs approximated as “infinite” in horizontal  
360           plane (e.g., Wang, 2000), with respect to the fault zone horizontal cross-section. Since we  
361           are using a one-dimensional model, such approximation is valid for our study area where

the Dead Sea is large enough in a horizontal plane (100 km x 10 km) compared to the thickness of the underlying strike-slip fault (cross-section) located in the central part of the valley.

Our results demonstrate that a fairly simple forward model (based on 1D analytical solution, Belfer et al., 2018) achieves a very good correlation between WLs and RIs of late-to-strong earthquakes on the Dead Sea fault. Whereas the fault system along the Dead Sea fault is more complicated, three-dimensional modeling of the tectonic motion, coupled to the pressure evolution, may give more reliable predictions regarding the earthquake ruptures and chronology. Finally, we note that under the man-induced decline of WL and RI changes presented in this article, with the current eustatic decrease in the Dead Sea level (at an average annual rate of  $\sim 1 \text{ m yr}^{-1}$ ), a late-to-large-severe earthquake will not be triggered by the mechanism discussed here. This not only presents the existence of a connection between WL and RI, but also provides additional guidance based on this connection, also about the uncertainties regarding the two phenomena separately.

## ACKNOWLEDGMENTS

This project was supported by the grants from Ministry of Natural Infrastructures, Energy and Water Resources of Israel # 213-17-002, and GIF- German - Israeli Foundation for Scientific Research and Development # I-1280-301.8. The data for this paper was obtained with analytical numerical modeling.

## Formatted: Header & Footer

**Formatted:** None

**Formatted:** None, **Font color:** Auto

**Formatted:** Body A, Indent: First line: 1.27 cm, Space Before: 6 pt, After: 0 pt

**Formatted:** None

### Formatted: Body A

**Formatted:** Hyperlink,0, Font: Not Italic

**Formatted: Centered**

382 **REFERENCE**

383 Agnon A. 2014. Pre-instrumental earthquakes along the Dead Sea rift. In Dead Sea transform fault  
384 system: reviews, edited by Garfunkel, Zvi, Ben-Avraham, Zvi, Kagan, Elisa, 207-261,  
385 Springer, Dordrecht. [https://doi.org/10.1007/978-94-017-8872-4\\_8](https://doi.org/10.1007/978-94-017-8872-4_8).

386 Ambraseys, N. 2009. Earthquakes in the Mediterranean and Middle East: a multidisciplinary study  
387 of seismicity up to 1900. Cambridge University Press. doi:  
388 <https://doi.org/10.1017/CBO9781139195430>

389 Ambraseys, N. N., Melville, C. P. and Adams, R. D. 1994. *The Seismicity of Egypt, Arabia and*  
390 *the Red Sea: A Historical Review*. Cambridge: Cambridge Univ. Press.  
391 <https://doi.org/10.1017/S1356186300007240>

392 Amiran, D. H., Arieh, E., and Turcotte, T. 1994. Earthquakes in Israel and adjacent areas:  
393 macroscopic observations since 100 B.C.E. *Israel Exploration Journal*, 44, 260– 305.  
394 <http://www.jstor.org/stable/27926357>.

395 Anderson, E. M. (1951). The dynamics of faulting and dyke formation with applications to Britain.  
396 Oliver and Boyd Avni, R., Bowman, D., Shapira, A. and Nur, A. 2002. Erroneous  
397 interpretation of historical documents related to the epicenter of the 1927 Jericho  
398 earthquake in the Holy Land. *Journal of seismology*, 6(4), 469-476.  
399 <https://doi.org/10.1023/A:1021191824396>

400 Baer G., G. J. Funning, G. Shamir, T. J. Wright (2008). The 1995 November 22, Mw 7.2 Gulf of  
401 Elat earthquake cycle revisited, *Geophysical Journal International*, 175(3), 1040-  
402 1054. <https://doi.org/10.1111/j.1365-246X.2008.03901.x>

403 Belfermer, M., Katsman, R. and Agnon, A. 2018. Effect of large-scale surface water level  
404 fluctuations on earthquake recurrence interval under strike-slip faulting. *Tectonophysics*,

**Formatted:** Header & Footer

**Formatted:** German (Germany)

**Formatted:** Body A

**Formatted:** Hyperlink.8, Font:

**Formatted:** None

**Formatted:** Hyperlink.9, Font:

**Formatted:** None, Font: (Default) Times New Roman

**Formatted:** Hyperlink.0, Font: (Default) Times New Roman

**Formatted:** None, Font: (Default) Times New Roman, Not Italic

**Formatted:** Hyperlink.0, Font: (Default) Times New Roman

**Formatted:** None, Font: (Default) Times New Roman

**Formatted:** Hyperlink.10, Font: Text Outline

**Formatted:** Body A

**Formatted:** Hyperlink.8, Font:

**Formatted:** Hyperlink.8, Font:

**Formatted:** Hyperlink.9, Font:

**Formatted:** Hyperlink.11

**Formatted:** Hyperlink.11

**Formatted:** Complex Script Font: Times New Roman, Hebrew

**Formatted:** Hyperlink.11

**Formatted:** Hyperlink.12, Font: (Default) Times New Roman, 12 pt, Not Bold, Not Italic, Font color: Black

**Formatted:** None, Font: (Default) Times New Roman, Font color: Black

**Formatted:** Body A

**Formatted:** Hyperlink.0, Font: Not Italic

**Formatted:** Centered

405 744, 390-402.

Formatted: Header & Footer

406 <https://doi.org/10.1016/j.tecto.2018.06.004>

407 Ben-Menahem, A. 1979. Earthquake catalogue for the Middle East (92 BC-1980 AD). *Boll. Geofis. Teor. Appl.*, 21, 245-313.

Formatted: Hyperlink.11

408 Bookman, R., Enzel, Y., Agnon, A., and Stein, M. 2004. Late Holocene lake levels of the Dead Sea. *Geological Society of America Bulletin* 116, 555-571.

Formatted: None

Formatted: Hyperlink.11

409 410 <https://doi.org/10.1130/B25286.4>

Formatted: Hyperlink.0, Font: Not Italic

411 412 Byerlee, J.D., 1978. Friction of rocks. In: Byerlee, J.D., Wyss, M. (Eds.), *Rock Friction and Earthquake Prediction*. Springer, Birkhäuser, Basel, pp. 615-626.

Formatted: Font color: Black

<https://doi.org/10.1007/978-3-0348-7182-2>

Formatted: Hyperlink.0, Font: Not Italic, Font color: Black

Formatted: Font color: Black

Formatted: None, Font color: Black

Formatted: Hyperlink.14, Font: (Default) Times New Roman, 12 pt, Not Bold, Not Italic, Font color: Black, Border: : (No border), Pattern: Clear

Formatted: Hyperlink.0, Font: Not Italic

Formatted: Hyperlink.15, Font: Not Bold, Not Italic, Font color: Black, Pattern: Clear

413 414 415 416 417 418 419 Durá-Gómez, I. and Talwani, P. 2010. Reservoir-induced seismicity associated with the Itoiz Reservoir, Spain: a case study, *Geophysical Journal International*, 181, 343-356.

<https://doi.org/10.1111/j.1365-246X.2009.04462.x>

Formatted: Hyperlink.0, Font: Not Italic

Elad, A. 1982. An early arabic source concerning the markets of Jerusalem. *Cathedra*, 24, 31-40.

420 421 422 Elad, A., 1992. Two Identical Inscriptions From Jund Filastin From the Reign of the Abbāsid Caliph, Al-Muqtadir. *Journal of the Economic and Social History of the Orient*, 35(4), 301-360. <https://doi.org/10.2307/3632739>

Formatted: Hyperlink.0, Font: Not Italic

423 424 425 Garfunkel, Z., 2014. Lateral motion and deformation along the Dead Sea Transform. In: Garfunkel, Z., Ben-Avraham, Z., Kagan, E. (Eds.), *Dead Sea Transform Fault System: Reviews*. 5. Springer, Dordrecht, pp. 109-150. <http://dx.doi.org/10.1007/978-94-017-8872-4>.

Formatted: Hyperlink.0, Font: Not Italic

426 Gerber, H., 1998. " Palestine" and Other Territorial Concepts in the 17th Century. *International*  
427 *Journal of Middle East Studies*, 30(4), 563-572. <https://www.jstor.org/stable/164341>

428 Guidoboni, E., Comastri, A., and Traina, G. 1994. Catalogue of Ancient Earthquakes in the  
429 Mediterranean Area Up to the 10th Century. Rome: Istituto nazionale di geofisica.  
430 <https://doi.org/10.1163/182539185X01377> <https://doi.org/10.1163/182539185X01377>

431 Guidoboni, E. and Comastri, A. 2005. Catalogue of Earthquakes and Tsunamis in the  
432 Mediterranean Area from the 11th to the 15th Century. Istituto nazionale di geofisica e  
433 vulcanologia.  
434 <https://doi.org/10.1515/BYZS.2008.854> <https://doi.org/10.1515/BYZS.2008.854>

435 Gupta, H., K., 2018, Reservoir triggered seismicity (RTS) at Koyna, India, over the past 50  
436 yrs. *Bulletin of the Seismological Society of America* 108.5B: 2907-2918.  
437 <https://doi.org/10.1785/0120180019>

438 Hamiel, Y., Masson, F., Piatibratova, O., & Mizrahi, Y. (2018). GPS measurements of crustal  
439 deformation across the southern Arava Valley section of the Dead Sea Fault and  
440 implications to regional seismic hazard assessment. *Tectonophysics*, 724, 171-178.  
441 <https://doi.org/10.1016/j.tecto.2018.01.016>

442 Hamiel, Y., & Piatibratova, O. (2019). Style and distribution of slip at the margin of a pull-apart  
443 structure: Geodetic investigation of the Southern Dead Sea Basin. *Journal of Geophysical*  
444 *Research: Solid Earth*, 124(11), 12023-12033. <https://doi.org/10.1029/2019JB018456>

445 Hofstetter, R., Klinger, Y., Amrat, A. Q., Rivera, L., & Dorbath, L. (2007). Stress tensor and focal  
446 mechanisms along the Dead Sea fault and related structural elements based on

Formatted: Header & Footer

Formatted: Hyperlink.11

Formatted: Body A

Formatted: Hebrew

Formatted: None, Underline color: Custom Color(RGB(60,60,60))

Formatted: Hebrew

Field Code Changed

Formatted: Hyperlink.17, Font: Not Bold, Not Italic, Font color: Black, Border: : (No border), Pattern: Clear

Formatted: Hyperlink.15

Formatted: Centered

447 seismological data. *Tectonophysics*, 429(3-4), 165-181.  
448 <https://doi.org/10.1016/j.tecto.2006.03.010>

449 Hua, W., Chen, Z. and Zheng, S., 2013a. Source parameters and scaling relations for reservoir-induced seismicity in the Longtan reservoir area. *Pure Appl. Geophys.* 170, 767-783.

450 <https://doi.org/10.1007/s00024-012-0459-7>

451 Hua, W., Chen, Z., Zheng, S., and Yan, C., 2013b. Reservoir-induced seismicity in the Longtan reservoir, southwestern China. *J. Seismol.* 17 (2), 667-681.

452 <https://doi.org/10.1007/s10950-012-9345-0>

453 Hough S. E. and Avni R., 2011. The 1170 and 1202 CE Dead Sea Rift earthquakes and long-term magnitude distribution of the Dead Sea Fault Zone, *Isr. J. Earth Sci.*, 58, 295-308.

454 <https://doi.org/10.1560/IJES.58.3-4.295>

455 Jaeger, J. C., Cook, N. G., & Zimmerman, R. (2009). *Fundamentals of rock mechanics*. John Wiley and Sons.

456 Kagan, E., Stein, M., Agnon, A., and Neumann, F. 2011. Intrabasin paleoearthquake and quiescence correlation of the late Holocene Dead Sea. *Journal of Geophysical Research: Solid Earth*, 116(B4). <https://doi.org/10.1029/2010JB007452>

457 Ken-Tor, R., Agnon, A., Enzel, Y., Stein, M., Marco, S., and Negendank, J. F. 2001. High-resolution geological record of historic earthquakes in the Dead Sea basin. *Journal of Geophysical Research-Solid Earth*, 106, 2221-2234.

458 <https://doi.org/10.1029/2000JB900313>

459 Klinger, Y., Le Béon, M. and Al-Qaryouti, M., 2015. 5000 yr of paleoseismicity along the southern Dead Sea fault. *Geophys. J. Int.* 202 (1), 313-327. <https://doi.org/10.1093/gji/ggv134>

460 Formatted: Header & Footer

461 Formatted: Body A

462 Formatted: Hyperlink.19, Font: Not Bold, Not Italic, Font color: Black, Pattern: Clear

463 Formatted: Hyperlink.19, Font: Not Bold, Not Italic, Font color: Black, Pattern: Clear

464 Formatted: Hyperlink.19, Font: Not Bold, Not Italic, Font color: Black, Pattern: Clear

465 Formatted: Hyperlink.19, Font: Not Bold, Not Italic, Font color: Black, Pattern: Clear

466 Formatted: Hyperlink.11

467 Formatted: Body A

468 Formatted: Hyperlink.11

469 Formatted: Hyperlink.8, Font: Not Bold, Not Italic, Font color: Black, Pattern: Clear

470 Formatted: Hyperlink.0, Font: Not Italic

471 Formatted: None

472 Formatted: Hyperlink.19, Font: Not Bold, Not Italic, Font color: Black, Pattern: Clear

473 Formatted: Hyperlink.19

474 Formatted: Hyperlink.11

475 Formatted: Hyperlink.8, Font: Not Bold, Not Italic, Font color: Black, Pattern: Clear

476 Formatted: Hyperlink.0, Font: Not Italic

477 Formatted: Body A

478 Formatted: Hyperlink.11

479 Formatted: Hyperlink.8, Font: Not Bold, Not Italic, Font color: Black, Pattern: Clear

480 Formatted: Hyperlink.0, Font: Not Italic

481 Formatted: Hyperlink.9, Font: Not Bold, Not Italic, Font color: Black, Pattern: Clear

482 Formatted: Centered

469 Langgut, D., Yannai, E., Taxel, I., Agnon, A. and Marco, S., 2015. Resolving a historical  
470 earthquake date at Tel Yavneh (central Israel) using pollen seasonality. *Palynology*, 40(2),  
471 145-159. <https://doi.org/10.1080/01916122.2015.1035405>

472 Lefevre, M., Klinger, Y., Al-Qaryouti, M., Le Béon, M. and Moumani, K., 2018. Slip deficit and  
473 temporal clustering along the Dead Sea fault from paleoseismological investigations. *Sci.  
474 Rep.* 8 (1), 4511. <https://doi.org/10.1038/s41598-018-22627-9>

475 Lyakhovsky, V., Ben-Zion, Y., Agnon, A., 2001. Earthquake cycle, fault zones, and seismicity  
476 patterns in a rheologically layered lithosphere. *J. Geophys. Res. Solid Earth* 106 (B3),  
477 4103–4120.

478 Marco, S., Stein, M., Agnon, A., and Ron, H. 1996. Long-term earthquake clustering: A 50,000-  
479 year paleoseismic record in the Dead Sea Graben. *Journal of Geophysical Research: Solid  
480 Earth*, 101(B3), 6179-6191. <https://doi.org/10.1029/95JB01587>

481 Masson, F., Hamiel, Y., Agnon, A., Klinger, Y. and Deprez, A., 2015. Variable behavior of the  
482 Dead Sea Fault along the southern Arava segment from GPS measurements. *comptes  
483 rendus geoscience*, 347(4), pp.161-169. <https://doi.org/10.1016/j.crte.2014.11.001>

484 Migowski, C., Agnon, A., Bookman, R., Negendank, J. F., and Stein, M. 2004. Recurrence pattern  
485 of Holocene earthquakes along the Dead Sea transform revealed by varve-counting and  
486 radiocarbon dating of lacustrine sediments. *Earth and Planetary Science Letters*, 222, 301–  
487 314. <https://doi.org/10.1016/j.epsl.2004.02.015>

488 Migowski, C., Stein, M., Prasad, S., Negendank, J. F. W., and Agnon, A. 2006. Holocene climate  
489 variability and cultural evolution in the Near East from the Dead Sea sedimentary record.  
490 *Quaternary Research*, 66(3), 421-431. <https://doi.org/10.1016/j.yqres.2006.06.010>

491 Palano, M., Impresia, P., & Gresta, S. (2013). Current stress and strain-rate fields across the Dead  
492 Sea Fault System: Constraints from seismological data and GPS observations. *Earth and*  
493 *Planetary Science Letters*, 369, 305-316. <https://doi.org/10.1016/j.epsl.2013.03.043>

494 Pandey, A.P. and Chadha, R.K., 2003. Surface loading and triggered earthquakes in the Koyna-  
495 Warna region, western India. *Phys. Earth Planet. Inter.*, 139 (3-4), 207-223.  
496 <http://dx.doi.org/10.1016/j.pepi.2003.08.003>

497 Parker, S.T., 1982. Preliminary Report on the 1980 Season of the Central" Limes Arabicus"  
498 Project. *Bulletin of the American Schools of Oriental Research*, 247(1), pp.1-26.  
499 <https://www.journals.uchicago.edu/doi/10.2307/1356476>

500 Rao, N. P., & Shashidhar, D. (2016). Periodic variation of stress field in the Koyna-Warna  
501 reservoir triggered seismic zone inferred from focal mechanism  
502 studies. *Tectonophysics*, 679, 29-40. <https://doi.org/10.1016/j.tecto.2016.04.036>

503 Russell, K. W., 1985. The earthquake chronology of Palestine and northwest Arabia from the 2nd  
504 through the mid-8th century AD. *Bulletin of the American Schools of Oriental*  
505 *Research*, 260(1), 37-59. <https://doi.org/10.2307/1356863>

506 Sadeh, M., Hamiel, Y., Ziv, A., Bock, Y., Fang, P., Wdowinski, S., 2012. Crustal deformation  
507 along the Dead Sea Transform and the Carmel Fault inferred from 12 years of GPS  
508 measurements. *J. Geophys. Res. Solid Earth* 117, B08410.  
509 <http://dx.doi.org/10.1029/2012JB009241>.

510 Scholz, C. H. (1972). Crustal movements in tectonic areas. *Tectonophysics*, 14(3-4), 201-217.  
511 [https://doi.org/10.1016/0040-1951\(72\)90069-8](https://doi.org/10.1016/0040-1951(72)90069-8)

Formatted: Header & Footer

Formatted: Body A

Formatted: Hyperlink.11

Formatted: Hyperlink.13, Font: Not Bold, Not Italic  
Formatted: None, Underline color: Blue, Font color: Blue

Formatted: Hyperlink.18, Font: Not Bold, Not Italic, Font color: Black  
Formatted: Hyperlink.18

Formatted: Centered

512 Pandey, A.P. and Chadha, R.K., 2003. Surface loading and triggered earthquakes in the Koyna  
513 Warne region, western India. *Phys. Earth Planet. Inter.* 139 (3-4), 207-223.  
514 <http://dx.doi.org/10.1016/j.pepi.2003.08.003>

515 Shapira, A., Avni, R., and Nur, A. 1993. A new estimate for the epicenter of the Jericho earthquake  
516 of 11 July 1927. *Isr. J. Earth Sci.* 42(2), 93-96.

517 Simpson, D. W. (1976). Seismicity changes associated with reservoir loading. *Engineering  
518 Geology*, 10(2-4), 123-150. [https://doi.org/10.1016/0013-7952\(76\)90016-8](https://doi.org/10.1016/0013-7952(76)90016-8)

519 Simpson, D. W., Leith, W., and Scholz, C. 1988. Two types of reservoir-induced seismicity. *Bulletin of the Seismological Society of America*, 78, 2025-2040.

520 Snow, D. T. (1982). Hydrogeology of induced seismicity and tectonism: Case histories of Kariba  
521 and Koyna. *Geological Society of America Special Papers*, 189, 317-360.  
522 <https://doi.org/10.1130/SPE189-p317>

523 Stern, O. 2010. Geochemistry, Hydrology and Paleo-Hydrology of Ein Qedem Spring System;  
524 Report GSI/17/2010; Geological Survey of Israel: Jerusalem, Israel, 2010; p. 91. (In  
525 Hebrew)

526 Talwani, P., 1997. On the nature of reservoir-induced seismicity. *Pure Appl. Geophys.* 150, 473-  
527 492. [https://doi.org/10.1007/978-3-0348-8814-1\\_8](https://doi.org/10.1007/978-3-0348-8814-1_8)

528 Wang, H., 2000. *Theory of Linear Poroelasticity With Applications to Geomechanics and  
529 Hydrogeology*. University Press, Princeton.

530 Wechsler, N., Rockwell, T. K., Klinger, Y., Štěpančíková, P., Kanari, M., Marco, S., & Agnon, A.  
531 (2014). A paleoseismic record of earthquakes for the Dead Sea transform fault between the

Formatted: Header & Footer

Formatted: Body A

Formatted: Hyperlink.11

Formatted: Hyperlink.13, Font: Not Bold, Not Italic

Formatted: None, Underline color: Blue, Font color: Blue

Formatted: Hyperlink.11

Formatted: Hyperlink.11

Formatted: Hebrew

Formatted: Body A

Formatted: Hyperlink.22

Formatted: Hyperlink.0, Font: Not Italic

Formatted: Hyperlink.22

Formatted: Body A

Formatted: Hyperlink.11

Formatted: Hyperlink.11

Formatted: Hyperlink.22

Formatted: Hyperlink.13, Font: Not Bold, Not Italic

Formatted: Centered

533 | **Formatted:** Header & Footer

533 | first and seventh centuries CE: Nonperiodic behavior of a plate boundary fault. *Bulletin of*  
534 | *the Seismological Society of America*, 104(3), 1329-1347. <https://doi.org/10.1785/0120130304>

535 | Williams, J. B., Schwab, M. J., & Brauer, A. 2012. An early first-century earthquake in the Dead  
536 | Sea. *International Geology Review*, 54(10), 1219-1228.  
537 | <https://doi.org/10.1080/00206814.2011.639996>

538 | **Formatted:** None, Underline color: Custom Color(RGB(34,34,34))

539 | **Formatted:** Body A

540 | **Formatted:** None, Underline color: Custom Color(RGB(34,34,34)), Hebrew

541 | **Formatted:** None, Font: (Default) Times New Roman, Underline color: Dark Gray

542 | **Formatted:** Hyperlink.13, Font: Not Bold, Not Italic

## 542 | Appendix: The earthquake history of the Dead Sea environs

543 | Numerous publications list earthquakes that hit the Dead Sea and its surroundings during the last  
544 | two millennia (e.g. Agnon, 2014; Ambraseys et al., 1994; Ambraseys, 2009; Amiran et al., 1994;  
545 | Guidoboni et al., 1994, Guidoboni and Comastri, 2005). In Belferan et al. (2018) we adopted  
546 | from the scores of listed events only the most destructive ones, typically causing local intensities  
547 | of VII or higher in Jerusalem. For a minimal epicentral distance of 30 km, this would translate to  
548 | a magnitude of ~5.7 or higher (according to the attenuation relation of Hough and Avni, 2011).

549 | **Formatted:** Hyperlink.22

550 | **Formatted:** Body A

551 | Table A1 lists the Dead Sea earthquakes considered for stress release across the Dead Sea basin  
552 | during the last two millennia. We used two criteria: noticeable damage in fortified Jerusalem, and  
553 | seismites in the northern Dead Sea. Our simple model simulates an earthquake time series, given  
554 | a water level curve. Eleven events from this time series correlate with events of magnitude ~6 or  
555 | more in the historic record. Yet, the model generates four events that are not included in our

556 | **Formatted:** Hyperlink.11

557 | **Formatted:** None, Complex Script Font: Times New Roman

558 | **Formatted:** Hyperlink.11

559 | **Formatted:** Centered

554 original [Histcatalog](#). On the other hand, a single event (~660 CE) listed in Belferman et al. (2018)  
555 has no counterpart in the simulations despite a wide range of level curves tested. All these curves  
556 are generated by a random number generator, subject to constraints from field data. We first  
557 discuss the four events required by the simulations one by one. Then we [review](#) the ~660 CE event  
558 along with other historic events that were left out already in Belferman et al. (2018).

Formatted: Header & Footer

Formatted: Hyperlink.11

559 The earthquakes in Table 1 are classified according to the level of acceptance for being destructive  
560 in Jerusalem. The nine events of **Class C** are all consensual, also used by Belferman et al. (2018).  
561 These events appear in all [cataloguescatalogs](#) and lists, and need no further discussion. The six  
562 events of **Class A** are debated events, accepted in the present study. All earthquakes in this class  
563 are selected by simultaneously satisfying two criteria: (1) The acceptance regularizes the relation  
564 between recurrence intervals and lake level; (2) They are corroborated by evidence from seismites  
565 in the northern basin of the Dead Sea (Ein Feshkha and Ein Gedi sites, Fig.A1corroborate).

Formatted: None, Complex Script Font: Times New Roman

Formatted: Hyperlink.11

566 We chose the year **33** CE to start our simulations. While this earthquake did not cause a widespread  
567 damage, it was recorded in all three seismite sites (Kagan et al., 2011), with a maximum of decade  
568 uncertainty based on dating by counting lamina under the microscope (Migowski et al., 2004;  
569 Williams et al., 2012).

Formatted: Hyperlink.11

570 The second entry in Table A1, **~100** CE, refers to two decades of unrest. Migowski et al. (2004)  
571 identified a pair of seismites around 90 CE and 112 CE in the 'Ein Gedi Core. The corresponding  
572 sequences in Ein Feshkha and Ze'elim Creek are laminates, attesting to quiescence. A historical  
573 hiatus between the Roman demolition of Jerusalem and the erection of Ilya Capitolina in its stead  
574 (70-130 CE) preclude historical evidence. Although damage to the Masada fortress has been  
575 assigned to an earthquake **1712** CE.

Formatted: None

Formatted: Hyperlink.11

Formatted: None, Complex Script Font: Times New Roman

Formatted: Hyperlink.11

Formatted: Hyperlink.11

Formatted: None

Formatted: Hyperlink.11

Formatted: Hyperlink.22

Formatted: None

Formatted: Hyperlink.22

Formatted: Hyperlink.22

Formatted: None

Formatted: Hyperlink.22

Formatted: None

Formatted: Centered

576 Table A2 lists ten earthquakes that have been reported to damage around Jerusalem but are not  
577 required by our simulations. The seven events of **Class R** are the debated events, rejected here  
578 after discussion. The three **Class S** events were skipped altogether in that compilation of  
579 Ambraseys (2009).

580 Of the seven Class R events, the 7 June **659** CE earthquake was accepted by us in Belferan et al.  
581 (2018). The earthquake has been associated with destruction of the Euthymius monastery 10 km  
582 east of Jerusalem, but no damage in the town of Jerusalem has been unequivocally reported  
583 (Ambraseys, 2009). In Belferan et al. (2018) we included this event in the [listcatalog](#) of Dead  
584 Sea earthquakes, as Langgut et al. (2015) have located it on the center of the Jordan Valley segment  
585 of the transform (Figure A1). However, this interpretation neglected the possibility that the rupture  
586 could have been outside the hydrological effect of the Dead Sea basin. One of the lessons of our  
587 numerous simulations is that our model would not support triggering of this earthquake shortly  
588 (less than a century) before the mid-8th century crisis, when lake levels were dropping to the lowest  
589 point in the studied period (420 m bsl, [Fig-Figure](#) 1a). When rejecting the 659 CE event, the 419  
590 CE earthquake is the one preceding the mid-8th century crisis; the three century recurrence interval  
591 fits well the low lake level.

592 **1016** CE: The collapse of the Dome of the Rock was not explicitly attributed to an earthquake by  
593 the original sources, who found it [enigmatic](#) as well (Ambraseys, 2009).

594 **1644** CE: Ambraseys (2009) quoted a late Arab author, al-Umari, who reported collapse of houses  
595 and deaths of five persons in “the town of Filistin”. While Ambraseys has interpreted it probably  
596 to Jerusalem, it might refer to al-Ramla, the historical capital of the classical Filistin District, as in  
597 “al-Ramla, Madinat Filastin” (Elad, 1992, p335). Or, it is a mistranslation of “Bilad Filistin” which  
598 at that time started refer to the entire Holy Land district, without specifying a town (Gerber, 1998).

**Formatted:** Header & Footer

**Formatted:** Hyperlink.11

**Formatted:** None

**Formatted:** Hyperlink.11

**Formatted:** None, Complex Script Font: Times New Roman

**Formatted:** Hyperlink.11

**Formatted:** None

**Formatted:** None, Font: Not Bold, Complex Script Font: Times New Roman, Not Bold

**Formatted:** Hyperlink.11

**Formatted:** Hyperlink.11

**Formatted:** None

**Formatted:** Hyperlink.11

**Formatted:** None, Complex Script Font: Times New Roman

**Formatted:** Hyperlink.11

**Formatted:** Hyperlink.11

**Formatted:** Hyperlink.11

**Formatted:** None, Complex Script Font: Times New Roman

**Formatted:** Hyperlink.11

**Formatted:** None

**Formatted:** Hyperlink.11

**Formatted:** None

**Formatted:** Hyperlink.11

**Formatted:** None

**Formatted:** Hyperlink.22

**Formatted:** Centered

Formatted: Header & Footer

599 Jerusalem, at that time, was called Bayt el Maqdis or, as nowadays, al-Quds. The only report of an  
600 earthquake in Jerusalem around 1644 mentions horror but no structural damage - the 1643 CE  
601 event that Ambraseys (2009) tends to equate with the 1644 CE event. A seismite in Ein Gedi core  
602 can be correlated with this event (Migowski et al., 2004, Table 2, entry 6). Migowski et al. (2004)  
603 have identified the seismite with the 1656 earthquake that was felt in Palestine; Ambraseys' (2009)  
604 interpretation was not yet available for them.

605 **1656** CE: This event was strong in Tripoli and only felt in Palestine. Migowski et al. (2004)  
606 correlated it to a seismite based on deposition rates (no lamina counting for that interval). Given  
607 the 1644 CE entry of Ambraseys (2009), this interpretation should be revised, and the 1656 CE  
608 earthquake is not to be associated with any local rupture in the Dead Sea.

Formatted: None

Formatted: Hyperlink.22

Formatted: None, Font: (Default) Times New Roman

Formatted: Centered

609  
610  
611  
612

**Table A1: A catalog of earthquakes that could potentially damage Jerusalem. The classes denote the level of acceptance of damage to Jerusalem among the researchers: C - consensual; B - accepted by Belfer et al., 2018; A - amended here; R - rejected here.**

Year CE or Century (marked C)	C	Seismite	Reference	Comments
	I	correl. by site		
	a			
	s	Z E E		
	s	E G <sup>y</sup> F		
		† ○		
33	B	+, +, +	MI, K&, W&	Identified in all three seismite sites, varve-counted to 31 BCE
100~	B	~, 2	MI, AM	Seismites ~90 and ~112; questionable archaeologic evidence
~175	B	~, +, +	MI	A seismite; no historic or archeological support
363	C	~, ~, +	K&, A&	A seiche in the Dead Sea, a seismite at EF° (north Dead Sea)
419	C	+, +, +	KT/MI/K&	
551	A	+, +, +	PA, AM	
747/9,757	C	+, +, +	KT/MI/K&	
1033	C	?, +, +	KT/MI/K&	
~1150	A	+, ~, /	AM, K&	I <sub>0</sub> IX - Mar Elias (& Qasr al-Yahud) monasteries demolished
1293	C	+, +, +	K&	
1458	C	+, +, h	MI	
1546	C	/, +, i	MI	
1712	A	/, +, t	MI	A& / I <sub>0</sub> VII - "ruined three Turkish houses in Jerusalem"
1834	C	+, +, u	KT, MI	
1903	R	m, m, s	A&, AM	I <sub>0</sub> VII Mt. of Olives; several shocks, I <sub>0</sub> up to VII over a large area
1927	C	+, +	KT, MI	AV / I <sub>0</sub> VII-VIII in and around Jerusalem (I <sub>0</sub> 7.8 by GMPE)

613  
614  
615  
616  
617

**Table A1: A list**

618 **Table A2.** Events listed in some catalogs and subsequently skipped (Class S) or declined (Class D) by Ambraseys (2009), or  
 619 rejected (Class R) in the present study.

620 *of earthquakes that could potentially damage Jerusalem. The classes denote the level of acceptance of damage to Jerusalem  
 621 among the researchers: C = consensual; B = accepted by Belfer et al., 2018; A = amended here; R = rejected here.*

622 Abbreviations and notes:

624 <sup>†</sup>ZE – Ze’elim Creek; <sup>‡</sup>EG – Ein Gedi core; <sup>§</sup>EF – Ein Feshkha Nature Reserve

625 AM: Ambraseys, 2009; A&: Amiran et al., 1994; K&: Kagan et al., 2011; L&: Langgut et al.

626 2015; KT: Ken Tor et al., 2004; MI: Migowski et al., 2004; PA: Parker, 1982; W&: Williams et

627 al., 2012.

Year CE	C	Seismite correl. by site	Reference	Comments
1				
a				
s				
		Z E E		
		E G <sup>‡</sup> F		
		† ○		
~659	R	+	L&,AM	Jordan Valley, possibly over 65 km NE of Jerusalem
808	S	/ - ?	A&	
1016	D	? ? ?	AM,A&	Damage to the Dome of Rock, no specific reference to shaking
1042	S	+	BM	Syria, off the Dead Sea transform
1060	S		A&,SB	The roof of Al-Aqsa collapsed
1063	R	/ - +	A&,AM,SB	Syrian littoral
1068	D	+	AM	Neither of the two events can be associated with the Dead Sea
1105	D	? ? ?	A&,AM	“Strong” but “no damage recorded in the sources”
1114	D	+	A&,AM	1114 - no damage around the city, a swarm, Kingdom’s north
~1117	R	+	A&,AM	
1557	R		Am	Collapse in Jerusalem: a gun foundry, a forgery, an oven
1644	R	h +* h	Am	Some damage and death toll in Palestine, likely Seismite 6 of MI

1656	R	h	h	A&AM,SB	Tripoli VII, Palestine IV, MI misidentified with Seismite 6
1817	R			AM	Two churches damaged in Jerusalem, Holy Sepulchre affected
1870	S	2	h	AM	Mediterranean source

629 **Abbreviations and notes:**

630 <sup>†</sup>ZE - Ze' elim Creek; <sup>‡</sup>EG - Ein Gedi core; <sup>°</sup>EF - Ein-Feshkha Nature Reserve

631 AM: Ambraseys, 2009; A&: Amiran et al., 1994; K&: Kagan et al., 2011; L&: Langgut et al.

632 2015; KT: Ken-Tor et al., 2004; MI: Migowski et al., 2004; PA: Parker, 1982; W&: Williams et

633 al., 2012.

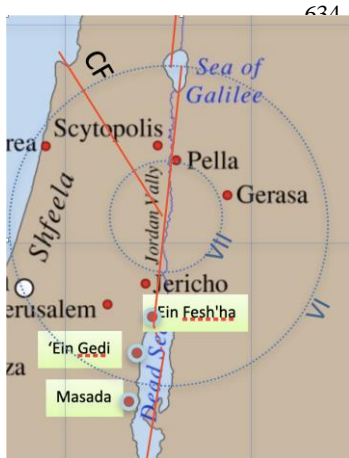


**Table A2:** Events listed in some catalogs and subsequently skipped (Class S) or declined (Class D) by Ambraseys (2009), or rejected (Class R) in the present study.

**Formatted:** Header & Footer

**Formatted:** None, Font: (Default) Times New Roman

**Formatted:** Font: (Default) Times New Roman

**Formatted**

**Formatted:** Table Style 2 A

**Formatted**

**Formatted**

**Formatted**

**Formatted**

**Formatted:** None, Font: (Default) Times New Roman

**Formatted:** Table Style 2 A

**Formatted:** Font: (Default) Times New Roman

**Formatted**

**Formatted:** None, Font: (Default) Times New Roman

**Formatted:** Table Style 2 A

**Formatted:** Font: (Default) Times New Roman

**Formatted**

**Formatted:** None, Font: (Default) Times New Roman

**Formatted:** Table Style 2 A

**Formatted:** Font: (Default) Times New Roman

**Formatted**

**Formatted**

**Formatted**

**Formatted**

**Formatted:** Hyperlink.22

**Formatted:** Body A

**Formatted:** Body A, Line spacing: Double

**Formatted:** Body A, Line spacing: single

**Formatted**

**Formatted:** Centered

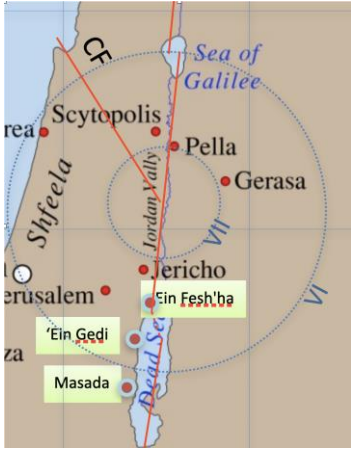


**Figure A1:** A map showing the epicenter reconstructed by Langgut *et al.* (2015) for the 659/660 mainshock.

**Formatted:** Header & Footer

**Formatted:** Body A

**Formatted:** None, Font: 9 pt

**Formatted:** Hyperlink, Font: 9 pt

**Formatted:** None, Font: 9 pt, Italic

**Formatted:** None, Font: 9 pt, Complex Script Font: Times New Roman, 9 pt, Hebrew

**Formatted:** None, Font: 9 pt, Italic

**Formatted:** None, Font: 9 pt, Complex Script Font: Times New Roman, 9 pt

**Formatted:** None, Font: 9 pt, Complex Script Font: Times New Roman, 9 pt

**Formatted:** None, Font: 9 pt, Hebrew

**Formatted:** None, Font: 9 pt, Italic

**Formatted:** Font: 9 pt

**Formatted:** Body A, Left, Indent: Before: 0 cm, First line: 0 cm, Space Before: 0 pt, After: 0 pt

**Formatted:** Centered